Journal of Materials Chemistry B

Accepted Manuscript

ROYAL SOCIETY OF CHEMISTRY

www.rsc.org/materialsB

Journal of Materials Chemistry B RSCPublishing

PAPER

Surface self-assembled hybrid nanocomposite with electroactive nanoparticle and enzyme confined in a polymer matrix for controlled electrocatalysis†

Cite this: DOI: 10.1039/xoxxoooooox

Received ooth March 2015,
Accepted ooth April 2015

DOI: 10.1039/xoxxoooooox

www.rsc.org/

Nan Zhu, Jens Ulstrup and Qijin Chi*

The three-dimensional network of highly branched poly(ethyleneimine) (PEI) is designed and synthesized on gold electrode surfaces. A self-assembled monolayer (SAM) of dithiobis (succinimidyl propionate) (DTSP) on the gold electrode was *first* prepared, which is confirmed by the reductive desorption of Au-S units. The PEI polymer was *then* covalently immobilized onto the DTSP layer, leaving free primary amine groups acting as a 3D skeleton for high loading of electroactive enzyme-size *Prussian* blue nanoparticles (PBNPs, 6 nm) via electrostatic trapping. Atomic force microscopy was used to disclose the microscopic structures of the different layers during the surface architecture formation. The resulting surface-bound nanostructured composite shows high electrochemical activity arising from confined PBNPs, and acts as an efficient electrocatalyst towards H_2O_2 reduction. Facile electron communication is achieved as reflected by a large electron transfer (ET) rate constant (k_s) of 200 s^{-1}, and the possible electron propagation mechanisms in the polymer network are discussed. This surface/interfacial nanocomposite can be further used in the accommodation of enzymes for electrochemical bio-catalysis. Glucose oxidase (GOD) was used towards this end, in a proof-of-concept study. This enzyme can be co-trapped in the PEI matrix and is interconnected with PBNPs, leading to highly efficient electrocatalyic oxidation and detection of glucose.

1. Introduction

Electrode-supported nanocomposites with specific functionality are of interest in the fields of sensors, heterogeneous catalysis and electrochemical energy technology. Surface self-assembly chemistry has played a vital role in the development of surface/interface derived nanostructures. For example, a self-assembled monolayer (SAM) with a selectively functional interface can provide a well-defined nanostructure for controlling the orientation of proteins and nanoparticles (NPs).[1-3] Such SAMs consisting of molecular nanoscale NPs or/and metalloproteins have come to offer not only desirable immobilization techniques, but also controlling interfacial electron transfer (ET) routes.[2] Controlled interfacial ET based on surface SAMs has been strikingly displayed for electroactive metalloproteins including representatives of the three major classes of ET proteins, i.e. heme proteins,[3,4] blue copper proteins,[5] and iron-sulphur proteins[6] as well as several redox metalloenzymes[7].

Because of its excellent electrocatalytic properties and high analytical sensitivity, *Prussian* blue (PB) has been thoroughly studied as an ET mediator in amperometric electrocatalysis,[8-11] and its electrochromic, photophysical, and magnetic properties addressed.[12,13] In a more general perspective, owing to their well-defined morphologies and controlled size, various electroactive NPs have been introduced as redox mediators for ET and electrocatalysis.[14,15]

SAMs of thiol-based molecules and metalloproteins assembled on electrode surfaces have also attracted growing interest.[16] Well-defined SAM nanostructures can be combined with electrochemically functional components, such as electroactive NPs and redox enzymes, into new composites for studying ET and electrocatalysis. Single-crystal electrodes with atomically planar surfaces such as Au (111) can further assist the control of molecular orientations for ET, improve the electrocatalytic activity, reduce the background signals, and facilitate high-resolution surface structural characterization. Such well-defined electrodes have been substrates for nanostructures addressed by *in situ* AFM and *in situ* scanning tunneling microscopy (STM) for a variety of molecular and biomolecular systems.[2,5,17-22]

PBNPs can also be immobilized on electrode surfaces via layer-by-layer SAMs, which provides a facile and versatile approach to creating a microenvironment for high loads of electrocatalytic centres as well as retaining their pristine nanostructure.[23-25] With their interconnected architecture and large surface area, which provide efficient mass transport to active sites, three-dimensional nanostructures self-assembled on electrode surfaces have attracted increasing attention.[26-28]

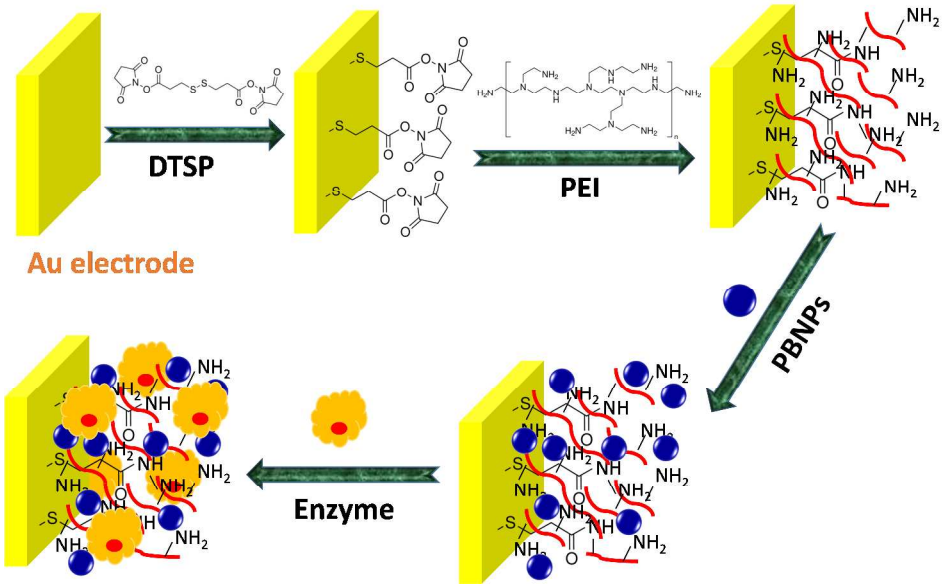

Fig. 1. Schematic diagram of an overall procedure for the construction of gold electrode-supported 3D nanocomposites. Not drawn to the scale.

In this context, polymer functionalized electrode surfaces have offered an effective platform for construction of electrochemical sensors and biosensors. For example, Pingarrón and co-workers have recently demonstrated that polyamidoamine based polymeric networks, which can combine with metallic nanoparticles and/or reduced graphene oxide (rGO), are very efficient matrices for immunization of enzyme and high-performance electrochemical biosensing.[29-32] In terms of combing PEI and PB, several previous reports[33-37] have shown that PEI-PB hybrids can act as a biocompatible network for confinement of enzymes and the resulting biosensors displayed high sensitivity and stability. In particular, Millner and co-workers showed that pre-impregnated PB screen printed carbon electrodes modified with PEI provided a cost-effective way for fabrication of lactate biosensors, which hold promising applications in diagnostic tests for intra-abdominal sepsis and anastomotic leak[34]. However, although electrodeposited PB films have been extensively studies since 1980s, the synthesis of PBNPs (50 nm) with defined and stable structure was not reported until 2002. To date, most reports in terms of PB material and PEI are about PB films and non-covalently coated PEI matrices on glass carbon electrodes. This study aims at synthesizing stable enzyme-size PBNPs (approximately 6 nm) and confining PBNPs in a 3D PEI matrix which is covalently bound to gold electrode surfaces.

In the present work, three-dimensional SAMs on single-crystal Au(111) electrode were used as a platform to confine PBNPs with a high loading for fast ET and electrocatalysis. The SAM nanostructures on Au(111) were characterized by electrochemistry and *in situ* AFM, and the ET features of the confined PBNPs are discussed. Dithiobis(succinimidyl propionate) (DTSP) is known as Lomant's reagent[38] and used as a protein or polymer cross-linking reagent by acylation of free primary or secondary aliphatic amino groups. Its terminal succinimidyl groups allow further covalent immobilization of biomolecular surface amino groups.[39] In this work a DTSP SAM was formed onto gold surfaces through the thiol-gold chemistry. This was followed by covalent binding of the primary amine-rich polymer PEI immobilizing the latter on top of the DTSP SAM. The covalent interaction between DTSP and PEI leaves a large number of free ammonium groups as a basis for a 3D terminal skeleton with a stable environment for a final step, in which high loads of PBNPs are electrostatically encapsulated. Fig. 1 shows a schematic diagram for the overall procedure for preparation of the 3D Au(111)-DTSP-PEI-PBNP nanostructure.

The surface-bound nanostructures were characterized by electrochemical reductive desorption of the Au-S units of the DTSP linker-based composites[40] and by AFM directly in the electrolyte solutions. The resulting 3D electrochemical DTSP/PEI/PBNP composite displays strong voltammetric PBNP signals and highly efficient electrocatalytic activity both towards reduction of H_2O_2 directly and towards oxidation of glucose in combination with immobilized glucose oxidase (GOD) on the surface of the 3D nanostructures. This three-dimensional structure also provides a simple and effective way to study the physicochemical nature of ET and electrocatalysis.

2. Experimental section

2.1 Materials and reagents

Dithiobis(succinimidyl propionate) (DTSP), potassium monohydrogen phosphate (K_2HPO_4, ≥ 99.999%), N, N-dimethylformamide (DMF), glucose oxidase (GOD, from *Aspergillus niger*, EC 1.1.3.4. 100000-250000 units g^{-1}), D-(+)-glucose (≥ 99.5%), Nafion® (5%), KCl (≥ 99%), $FeCl_3$ (≥ 99.5%) and $Fe(NO_3)_3$ (≥ 99.5%) were all from Sigma-Aldrich. Poly(ethyleneimine) (PEI) (MW = 750,000, 50% w/v in H_2O) was from Fluka. Potassium dihydrogen phosphate (KH_2PO_4, ≥ 99.5%), $K_4[Fe(CN)_6]$ (≥ 99%), KOH (≥ 99.995%) and H_2O_2 (30%) were from Merck, and $K_3[Fe(CN)_6]$ (≥ 99%) from Riedel-de Haën. All other reagents used were at least of analytical grade. 1 mM PEI was obtained by diluting the stock solution with PBS buffer. Milli-Q water (18.2 MΩ cm) was used throughout.

2.2 Synthesis of PBNPs

PBNPs were prepared in three steps. In the first step, solid PB pigment was synthesized as follows: $Fe(NO_3)_3$ (30 ml 1.3 M)

solution was gradually added to $K_4[Fe(CN)_6]$ (60 ml 0.5 M) solution under vigorous stirring. The mixture immediately changed color from yellow to dark blue. When mixing was complete, the reaction mixture was vigorously stirred for another 5 min. The resulting mixture was then washed with Milli-Q water and centrifuged at 4°C several times to remove the supernatant of unreacted reagents. The precipitate was collected and dried in air overnight.

In the second step, the PB pigment was redispersed by adding $K_4[Fe(CN)_6]\cdot 3H_2O$ into the pigment-water suspension. To achieve the water-soluble nanoparticles, solid PB pigment (0.4 g) was suspended in 15 ml water, followed by adding freshly prepared $K_4Fe(CN)_6]$ solution (5 ml 45 mM). The suspension was dissolved into a transparent dark blue solution after strong stirring for 4 h.

The third step was purification of the PBNP solution. Purification was performed by using a Stirred Ultrafiltration Cell and membrane to remove residual salts. The Stirred Ultrafiltration Cell was assembled and the PBNP solution added and diluted with Milli-Q water with the membrane 3000 according with the PBNP size. The process was repeated 3-5 times by adding fresh Milli-Q water until the filtrate was colourless. The As-synthesized PBNPs were systematically characterized, particularly with the HR-TEM image and size-distribution histogram provided in ESI Fig. S1.

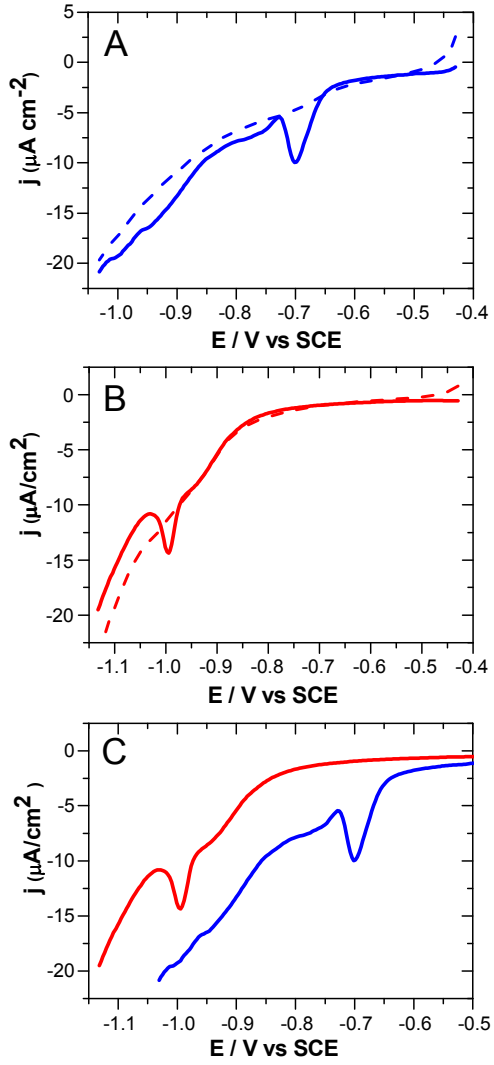

Fig. 2. (A) Linear scan voltammograms for reductive desorption of Au(111)-DTSP: the first scan (solid line) and the second scan (dotted line). (B) Linear scan voltammograms for reductive desorption of Au(111)-DTSP-PEI: the first scan (solid line) and the second scan (dotted line). (C) Comparison of linear scan voltammograms of reductive desorption of DTSP (blue line) and Au(111)-DTSP-PEI (red line) electrodes. Electrolyte: 0.5 M KOH solution; scan rate: 20 mV s^{-1}.

2.3 Preparation of self-assembled 3D nanostructures on the electrode surface

Single-crystal Au(111) electrodes, prepared as previously described[17,18] were used as working substrates in both electrochemistry and *in situ* AFM. The Au(111) electrodes were first annealed in a H_2 flame and then quenched in Milli-Qwater saturated with H_2 gas. The quenched Au(111) electrodes were immediately immersed into freshly prepared 5 mM DTSP DMF solutions and left overnight. After rinsing the samples first with DMF, and then several times with Milli-Q water, the gold electrodes were transferred into 1 mM PEI solution overnight. The SAM/PEI modified electrodes were transferred next into 5-6 nm PBNP solution at room temperature to form the 3D nanostructure.

2.4 Electrochemical and *in situ* AFM measurements

A three-electrode Autolab Electrochemistry System (Eco Chemie, The Netherlands) controlled by the general-purpose electrochemical system software was used to record cyclic voltammograms at room temperature (21±2 °C). Amperometric i-t response curves were recorded using a CHI 760 electrochemical workstation. SAM/PEI modified Au(111) electrodes were used as the working electrode (WE). The counter electrode (CE) was a coiled platinum wire, and the reference electrode (RE) a freshly prepared reversible hydrogen electrode (RHE). All potentials are referred to the saturated calomel electrode (SCE). The RHE potential was checked against a SCE after each measurement. Purified argon (5 N, Chrompack, Varian) was applied to purge dioxygen from electrolyte solutions before the measurements, and a gas stream maintained over the solution during the measurements. Electrolyte solutions consisting of 10 mM phosphate buffer and 0.1 M KCl (pH 7.0) were used throughout for all electrochemical measurements.

AFM imaging was carried out using a 5500 AFM System (Agilent Technologies) equipped with in-house made electrochemical cells. The tapping Mode was mostly used. Identical liquid environment conditions were used for *in situ* AFM and in electrochemistry.

3. Results and discussion

3.1 Preparation and characterization of surface polymeric nanostructures

SAM nanostructures were tracked through each step during the preparation process to define their properties. Voltammetry of the electrochemical reductive desorption of n-alkanethiol self-assembled monolayers (SAMs) from a metal surface in strongly alkaline solution has been widely used to diagnose the state of thiol-based SAMs and engineered SAMs,[2,40-42] since the first report by Porter and coworkers.[43,44] The systematic studies by Imabayashi et al. have revealed the quantative relationship of the intermolecular interaction between adsorbed thiol species of different alkyl chain lengths and the reductive desorption peak potential (E_p), indicating that E_p of variable-length alkanethiols is shifted negatively with increasing the alkyl chain length by about 15 mV per methylene group.[40]

The reductive desorption of different SAM layers for the thiol-bound Au(111)-DTSP and Au(111)-DTSP-PEI layers in 0.5 M KOH solution were addressed in this work and are compared in Fig. 2. A reductive desorption peak was observed around -0.7 V (vs. SCE) in the first scan for Au(111)-DTSP (Fig. 2A). This accords well with previous reports.[16,39,40] No reductive desorption peaks were detected in successive scans of either Au(111)-DTSP or Au(111)-DTSP-PEI (Fig. 2B and 2C), a clear indication of the irreversible nature of the reductive desorption at negative potentials. The Au(111)-DTSP-PEI system (Fig. 2B) displayed a reduction peak around -1.0 V (vs. SCE) in the first scan. This is significantly shifted towards negative potentials (about 30 mV) compared with the peak in the absence of polymer (Fig. 2C). The covalent bond between DTSP and PEI and the large molecular mass of PEI thus invokes similar behavior as increased alkanethiol chain lengths.

During this desorption process, the Au-S surface coverage of Au(111)-DTSP and Au(111)-DTSP-PEI was estimated as 2.1×10^{-10} and 1.3×10^{-10} mol cm^{-2}, respectively. The high Au-S coverage is associated with the high density of sulfur linking groups in the DTSP primary linker. The average distance between neighboring surface Au-S units in the DTSP adlayer (assuming for simplicity a square lattice) estimated from the reductive desorption peaks is thus 0.9 and 1.15 nm for Au(111)-DTSP and Au(111)-DTSP-PEI, respectively. These values can be compared with those for a $(\sqrt{3} \times 4)R30^o$ lattice of cysteamine (from *in situ* STM, two molecules per unit cell), viz. 5.7×10^{-10} mol cm^{-2} or an average intermolecular distance of 0.56 nm.[45] The $(3\sqrt{3} \times 6)R30^o$ cysteine lattice gives 4.0×10^{-10} mol cm^{-2} or an average distance of 1.2 nm.[18] The Au-S surface densities of the Au(111)-DTSP adlayers are thus in keeping with close to full monolayer packing of the Au-S linking units of the primary DTSP linker.

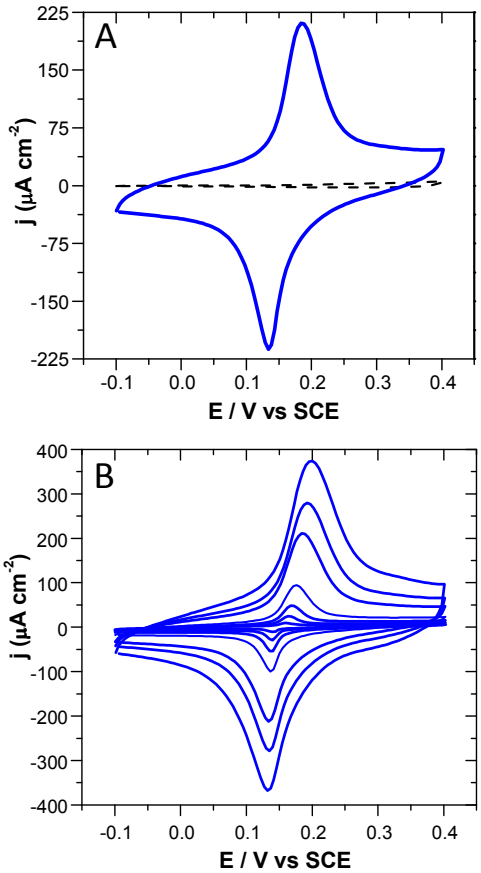

Fig. 3. (A) Comparison of CVs of Au(111)-DTSP-PEI-PBNPs (blue line) and Au(111)-DTSP-PEI (black dotted line) in 0.1 M KCl. Scan rate is 0.05 V s^{-1}. (B) Representative CVs of Au(111)-DTSP-PEI-PBNPs in 0.1 M KCl PBS solution (pH 7.0). Scan rates: 0.02, 0.05, 0.1, 0.2, 0.5, 0.7, 1.0 V s^{-1}.

3.2 Electron transfer behaviour of PBNPs confined in a polymer matrix

Fig. 3A compares the cyclic voltammograms (CVs) of Au(111)-DTSP-PEI-PBNPs and Au(111)-DTSP-PEI in the potential range from -0.1 to 0.4 V. No redox peaks were detected in the absence of PBNPs (black dotted line) but a strong pair of peaks around 0.15 V appeared for the Au(111)-DTSP-PEI-PBNP, caused by oxidation and reduction of the PBNPs. The oxidation peak is clearly shifted positively and the reduction peak negatively with increasing scan rates (Fig. 3B). To quantify the ET feature, we have shown the relationship between the peak current and scan rate (υ^x, x = 0.5, 0.6, 0.7, 0.8, 0.9, 1.0) by a series of plots (Fig. 4). The best linear fit is obtained with x =0.8-0.9, indicative of close to thin-layer voltammetric behavior, but the PBNPs diffusion within the polymer matrix still plays a role in determining the overall ET kinetics.[46] The best fitted exponent value, between one half and unity $0.5 < x < 1$, is likely to reflect thin-layer behaviour at low scan rate (x = 1) and diffusion-like behaviour at high scan rate (x = 0.5). We might expect that PBNPs would be more mobile in a hydrated and branched polymer matrix, but the electrostatic interaction appears to be strong enough to confine nanoparticles. We shall discuss this further below.

The ET rate constant (k_s) was calculated as 200 ± 10 s^{-1} (based on a one-ET process), according to the Laviron method.[3,47] This value appears large. In view of the three-dimensional high-density distribution of PBNPs in the PEI matrix, the rate constant must, however, necessarily accord with the notion of "apparent" and may involve both interfacial electrochemical ET between PBNPs and Au(111) electrode, and diffusion-like or percolative electron "hopping" between PBNPs in the DTSP/PEI matrix.

The PBNP voltammetric data shown in Figs.3 and 4 also offer a clue to the mechanism of interfacial electrochemical ET of the PBNPs in the confined Au(111)/DTSP/PEI environment. The following observations are notable:

(1) Only the PBNPs closest to the Au/polymer-matrix interface contribute directly to the current but electron supply from PBNPs in the whole matrix is obviously crucial. PBNP dynamics is therefore paramount.

(2) Voltammetric charge supply could be either by "vehicular diffusional motion of whole PBNPs or by ET ("hopping") between individual PBNPs. If the PBNP load is high, as in the system presently addressed, these two mechanisms display close to equivalent voltammetric behaviour by crude correlations between the PBNP diffusion coefficient in the matrix D_{matrix}, and the rate constant for ET (hopping) between pairs of PBNPs, k_{ET} in forms such as[48]

$$D_{matrix} \approx N <\delta>^2 k_{exch} \qquad (1)$$

where $<\delta>$ is the average diffusion jump length and N a geometric factor that represents the nearest neighbour number and orientation. For the ET mechanism to be effective, high hopping site (PBNP) concentration or small ET distances are required. Tunnelling and concentration factors are therefore of minor importance and therefore omitted in the crude coarse-grained form of eq.(1).

(3) Diffusion or diffusion-like behaviour is a rationale for the PBNP voltammetric behaviour observed. The non-orthodox correlation between the peak current density j_p and scan rate, v, vs. $j_p \propto v^{0.8}$ or $v^{0.9}$ substantiates that the diffusion/ET is in a confined matrix space in which the diffusion length is comparable to the thickness of the DTSP/PEI adlayer. The $j_p \propto v^{0.8\text{-}0.9}$ correlation is thus likely to reflect $j_p \propto v^{0.5}$ behaviour at high scan rate where the diffusion profile does not reach the outer DTSP/PEI edge, and $j_p \propto v$ behaviour at low scan rate where the profile reached the outer edge during each scan. The numerical $j_p \propto v^x$ ($0.5 < x < 1$) reflects this transition. Other cases of confined space diffusion or electron hopping in electrochemical systems are reported elsewhere[49-52]. Detailed theoretical treatments of spatially confined diffusion in electrochemical systems are also available[53-55].

3.3 AFM imaging of microscopic structures of 3D surface nanocomposites

The microscopic structures of different steps in the production of 3D SAM on ordered Au (111) electrodes were characterized by *in situ* AFM, in the same 0.1 M KCl PBS

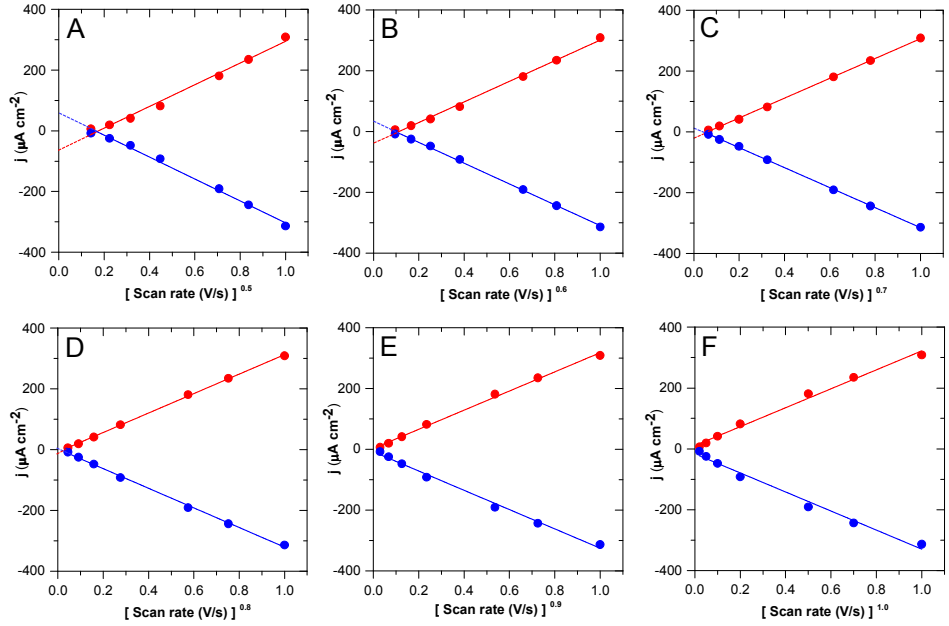

Fig. 4. A series of plots for uncovering the relationship between the peak currents (I_{pa} and I_{pc}) and scan rate (υ^x, x = 0.5, 0.6, 0.7, 0.8, 0.9 1.0). The best linear fit is obtained with x = 0.8-0.9.

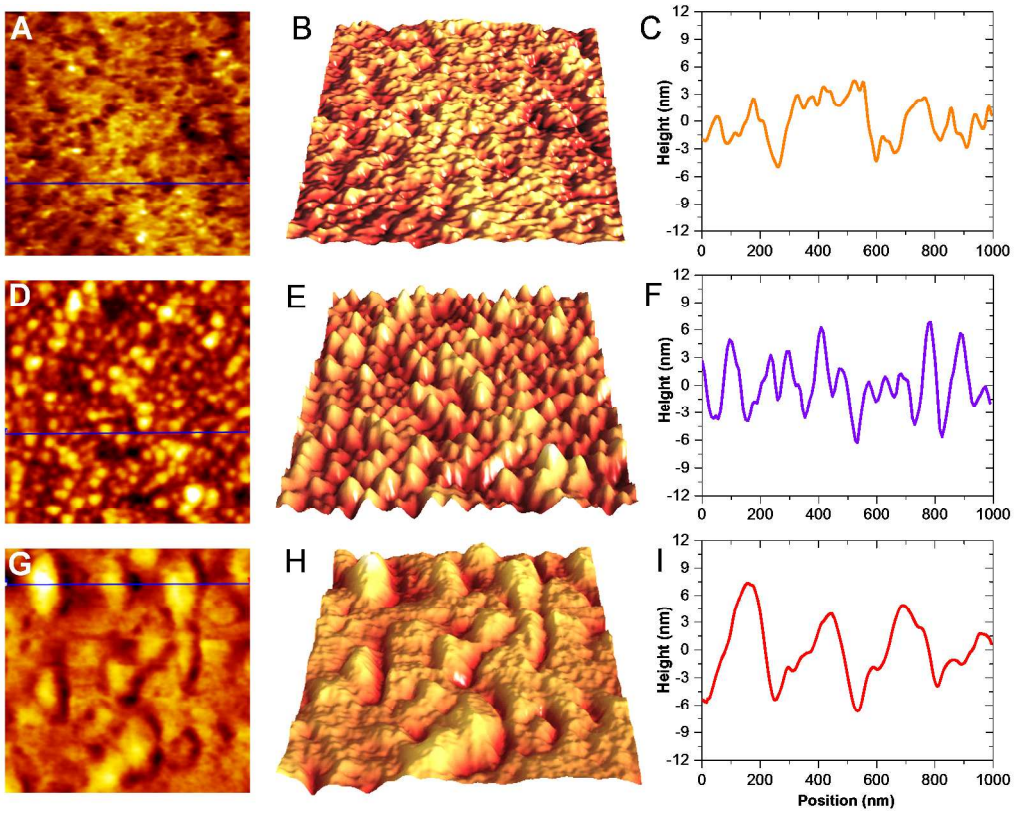

Fig. 5. *In situ* AFM images of SAM based nanostructures: (A) and (B) Au(111)-DTSP-PEI, (D) and (E) Au(111)-DTSP-PEI-PBNPs, (G) and (H) Au(111)-DTSP-PEI-PBNPs-GOD. (B), (E) and (H) are the 3D AFM images corresponding to (A), (D) and (G), respectively. (C), (F) and (I) are the cross-section profiles of the lines marked in (A), (D) and (G), respectively. All the images were recorded in liquid 0.1 M KCl PBS solution as used for electrochemical measurements. The scanned area of all the images is 1 x 1 μm^2.

buffer solution as for the electrochemical measurements. Fig. 5A and 5B show AFM images of immobilized PEI on Au(111)-DTSP in a randomly chosen area of 1 × 1 μm^2. The surface appears rough with three-dimensional nanostructures as seen from the cross-sectional profile (Fig 5C), and indicative that PEI covalently linked with DTSP on Au(111) offers a 3D skeleton for PBNP immobilization. The majority of the nanostructures observed when PBNPs were assembled on the Au(111)-DTSP-PEI surface (Fig. 5D and 5E), were single nanoparticles with little agglomeration. Importantly, the PBNP nanostructures seem to cover fully the PEI adlayer, with some 5-6 nm nanoparticles appearing outside and some inside the adlayers (Fig 4E), which was higher than pure PEI (Fig 5C). This high surface coverage of nanostructures offers highly efficient electrocatalysis. Fig. 5G and 5H show AFM images of the sample after immobilizing glucose oxidase (GOD) on the Au(111)-DTSP-PEI-PBNP surface. The small granular features are attributed to adsorbed GOD molecules. Some overlayers of enzyme are seen, although not covering uniformly the whole surface.[56] The crystallographic dimensions of a deglycosylated GOD molecule is reported to be 6.0 nm × 5.2 nm × 7.7 nm.[57] The apparent AFM size of native GOD (Fig. 5H and 5I) appears to be larger than its physical sizes, especially in liquid electrolyte environment partially due to the AFM convolution effect.[58] Although this enzyme-electrode topography does not tell us clear clues about enzyme activity towards glucose oxidation, AFM imaging in the liquid environment clearly reveals the presence of GOD confined stably in a surface polymeric matrix and available for electrocatalysis assays as described below.

3.4 Electrocatalysis and electrochemical bio-catalysis of surface hybrid nanocomposites towards targeted molecules

PB as electrochemical mediator for analytical applications has found wide use in the biosensor field in the past decades.[11] We have addressed the three-dimensional SAM PBNP nanostructures as catalytically efficient architectures towards electrocatalytic reduction of H_2O_2 and glucose as two broadly important biological metabolites. A significant electrocatalytic effect on 0.25 mM H_2O_2 reduction in the Au(111)-DTSP-PEI-PBNPs system is recorded in Fig. 6A (red line) compared with the adlayer without PBNPs assembled on the surface (Fig. 6A black line). Amperometric current (i)–time (t) responses of Au(111)-DTSP-PEI-PBNPs to successive additions of H_2O_2 at -0.05V was also acquired (red line, Fig. 6B).

The response was rapid and 95% of the steady-state current was reached within 5s. The current density for H_2O_2 reduction increases with increasing concentration. The calibration curve for the 3D SAM nanostructure showed a good linear response to the H_2O_2 concentration in the 0.3-30 mM range with the detection limit of 5 μM (Fig. 6C). The wide linear range indicates that high loading of active PBNPs has been achieved for the catalytic process. The H_2O_2 response on Au(111)-DTSP-PEI without PBNPs under the same conditions is displayed in Fig. 6B (black line) and Fig. 6C (black line) for comparison and

shows only a very weak response compared with the Au(111)-DTSP-PEI-PBNPs electrodes.

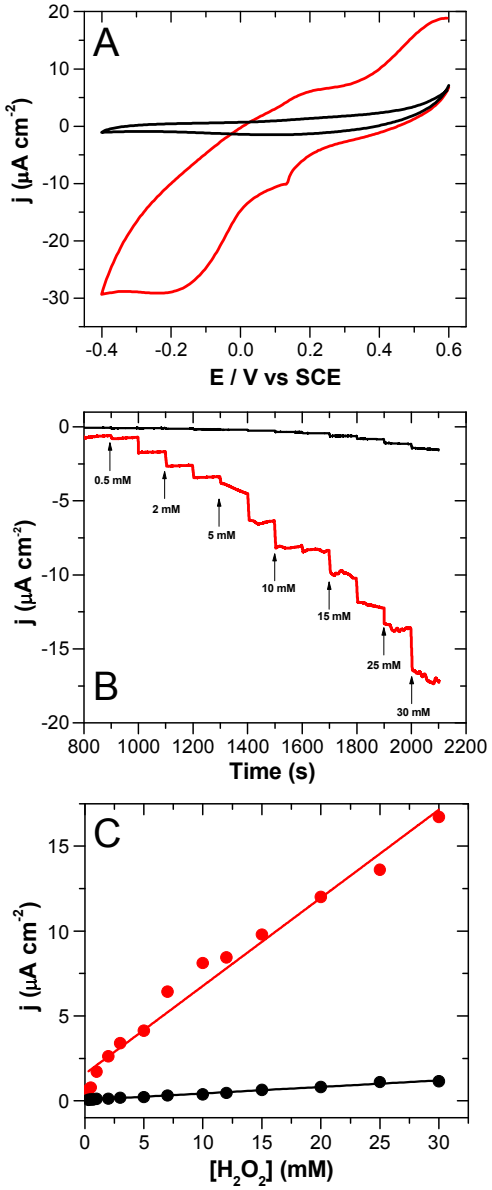

Fig. 6. (A) A comparison of electrocatalytic activity of Au(111)-DTSP-PEI-PBNPs (red curves) and Au(111)-DTSP-PEI (black curve) electrodes in the presence of 0.25 mM H_2O_2 . Scan rate 20 mV s^{-1}. (B) Amperometric response curves of Au(111)-DTSP-PEI-PBNPs (red) and without PBNPs (black) at an applied potential of -0.05 V vs SCE upon successive injection of different concentrations of H_2O_2 for each step under constant stirring and Ar saturation. Concentration from 0.3 to 30 mM H_2O_2. (C) The relationship between catalytic current density and concentration of H_2O_2 for Au(111)-DTSP-PEI-PBNPs (red) and without PBNPs (black). Electrolyte solution 0.1M KCl PBS (pH 7.0).

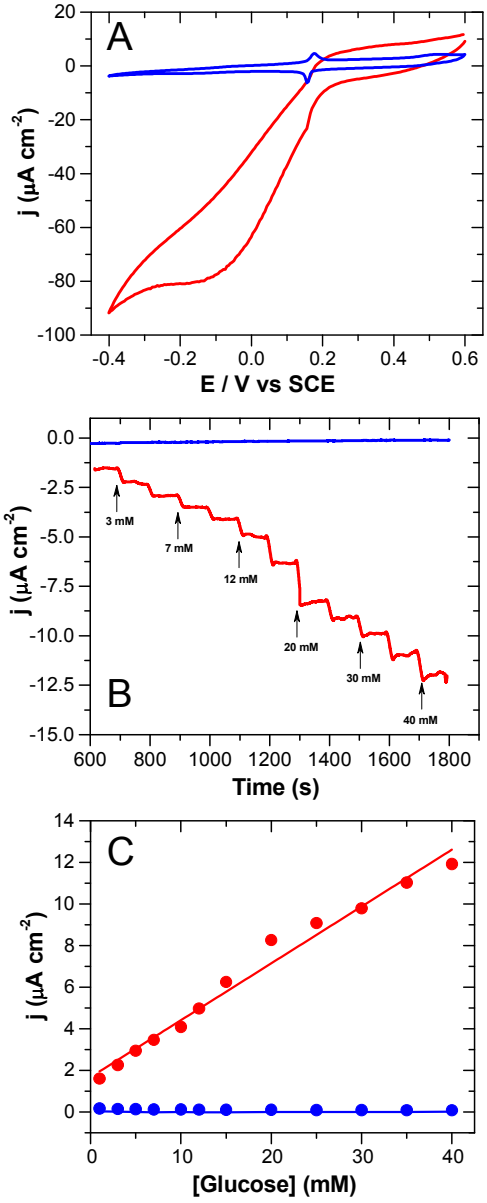

Fig. 7. (A) Comparison of electrocatalytic activity of Au(111)-DTSP-PEI-PBNPs-GOD-Nafion in 10 mM glucose solution with GOD (red) and without GOD (blue). Electrolyte solution 0.1M KCl PBS (pH 7.0), Scan rate 20 mV s^{-1}. (B) Amperometric response curve of Au(111)-DTSP-PEI-PBNPs-GOD-Nafion (red) and without GOD (blue) at a detection potential of -0.05 V vs. SCE upon successive injection of different concentrations of glucose for each step under constant stirring. Concentrations from 1 to 40 mM glucose. (C) Electrocatalytic activity relationship between catalytic current density and concentration of glucose for Au(111)-DTSP-PEI-PBNPs-GOD-Nafion (red) and without GOD (blue).

Electrocatalysis of glucose oxidation using this sensing element can be achieved by measuring the current for the reduction of hydrogen peroxide.[59] Au(111)-DTSP-PEI-PBNPs-GOD-Nafion was selected as working electrode for catalytic oxidation of glucose. Electrocatalysis is clearly observed after adding glucose in the electrolyte (Fig. 7A). Amperometric i-t responses of Au(111)-DTSP-PEI-PBNPs-GOD-Nafion to successive additions of glucose at the fixed potential of -0.05V (Fig. 7B, red line) show that the catalytic current density increases with increasing glucose concentration. The calibration curve for the 3D SAM nanostructures shows a good linear response to the glucose concentration in the range of 1-40 mM with the detection limit of 10 μM (Fig. 7C red line). This wide linear range can potentially be used in many contexts. The response without GOD was insignificant as demonstrated in

Fig. 7B (blue line) and Fig. 7C (blue line). The amperometric responses to H_2O_2 reduction and glucose addition are both very fast due to the interconnected 3D nanostructure. The high surface area of the 3D nanostructure that is also permeable to electrolyte thus appears to enhance significantly the sensing capacity towards H_2O_2 reduction and glucose oxidation compared to the corresponding 2D assemblies[60,61].

The electrochemical version of Michaelis–Menten equation (Eq. 2) was used to extract the kinetics characteristic of the electrocatalytic process by fitting the experimental data.[62]

$$j_{cat} = nF\Gamma \frac{k_{cat}[\mathrm{S}]}{K_M + [\mathrm{S}]} \qquad (2)$$

where j_{cat} is the electrocatalytic current density, [S] is glucose concentration, Γ is the surface PBNP coverage (estimated by electrochemical CVs), n the number of electrons transferred (here = 4), F the Faraday constant, K_M the apparent Michaelis constant, and k_{cat} the apparent catalytic turnover rate.

Fig. 7c can be best fit by Eq. 1 as shown in Fig. S2 (the solid curve) with the values of k_{cat} = 21 ± 3 s^{-1} and K_M = 29 ± 4 mM. The apparent K_M is relatively large, close to that for free GOD in homogeneous solutions. The k_{cat} is clearly smaller than the uncatalyzed PBNP electron transfer (ET) rate constant (200 s^{-1}). This must be attributed to different rate-determining steps. The uncatalyzed interfacial electrochemical ET of the PBNPs only involves the ET step itself, whereas the electrocatalytic efficiency is determined by concerted effects of interfacial ET involving both the PBNP/electrode contact and the PBNP/enzyme/glucose interaction. If the latter step is rate determining the observed interfacial electrochemical rate constant will be, expectedly quite different. Overall, the results suggest that the 3D nanostructure SAM provided a high surface coverage of redox mediator PBNPs for electrocatalysis, resulting in good response to high concentration of glucose with a relatively large value of K_M.

Finally, we have evaluated the stability of *Au(111)-DTSP-PEI-PBNPs-GOD-Nafion* electrodes. The two batches of experiments were carried out over a period of about two months, where the electrodes were stored at 4°C either in the dry state or in phosphate buffer (10 mM, pH 7.0). After 30 days, the electrocatalytic activity of the electrodes retained approximately 87% when the electrodes were kept in the dry state. The remained activity is less but still at 76%, when the electrodes were stored in buffer solutions. The electrocatalytic activity decreased to about 63% and 51% after 50 days, respectively, for the dry-state and solution storage. The lower stability in the solution storage mostly likely arises from the partial leakage of glucose oxidase from the PEI matrix, due to non-covalent but electrostatic confinement.

4. Conclusions

We have exploited surface self-assembly chemistry to prepare three-dimensional interfacial nanocomposites consisting of polymer matrix, electroactive nanoparticles and enzyme. Atomically planar single-crystal Au(111) electrodes were used to ascertain well-defined electrochemical microenvironments for the surface architecture and structural characterization with *in situ* AFM. A monolayer of dithiobis(succinimidyl propionate) (DTSP) on Au(111) was prepared and utilized for covalent immobilization of the primary amine-containing polymer Poly(ethyleneimine) (PEI). The PEI matrix enables to confine PBNPs in high load as well as offering a biologically friendly environment for further accommodation of enzymes. The confined PBNPs exhibit high electroactivity with a large interfacial ET rate (200 s^{-1}), leading to highly efficient electrocatalysis. Together with our previous attempts of two-dimensional alkanethiol immobilized PBNPs,[60,61] the three-dimensional Au(111)/DTSP/PEI/PBNP surface systems offer a new class of well characterized highly efficient substrates for electrocatalytic reduction of H_2O_2 alone and in combination with GOD for glucose oxidation. The method is therefore expected to be applicable to other redox enzymes immobilized in similar ways. Owing to controlled preparation of three-dimensional surface nanostructures, good stability, and high reproducibility, PBNP-based nanocomposites thus stand out as attractive interfacial materials for fabrication of electrocatalytic sensing devices, and provides a platform for probing ET features of electroactive NPs.

Finally, single-crystal gold electrodes were used in the present work to facilitate the surface characterization of nanostructures. However, the method is fully applicable to poly-crystalline metallic electrodes or any other electrode materials that enable thiol based self-assembly. For example, from an application point of view, both thin gold film (coated on glass or silicon wafer) electrodes and commercially available low-cost printed gold disc electrodes would appear to be highly suitable for the fabrication of practical sensing devices.

Acknowledgements

This work was supported by the Danish Research Council for Technology and Product Science (Project No. 12-127447) and the Lundbeck Foundation (Grant No. R49-A5331), N.Z. acknowledges the NanoScience Center at University of Copenhagen and Nano•DTU for a PhD fellowship.

Abbreviations

PBNPs, *Prussian* blue nanoparticles; PEI, poly(ethyleneimine); DTSP, dithiobis(succinimidyl propionate); GOD, glucose oxidase; SAM, self-assembled monolayer; ET, electron transfer; AFM, atomic force microscopy, SCE, saturated calomel electrode.

Notes and references

Department of Chemistry, Technical University of Denmark, DK-2800 Kongens Lyngby, Denmark. *E-mail: cq@kemi.dtu.dk; Phone: +45 45252032; Fax: +45 45883136.

† Electronic supplementary information (ESI) available: HRTM image and size-distribution histogram of PBNPs, and additional electrochemical data. See DOI: 10.1039/TB-ART-03-2015-000469

1 (a) Q. Chi, J. Zhang, P. S. Jensen, H. E. M. Christensen and J. Ulstrup, *Faraday Discussion* 2006, **131**, 181-195. (b) S. Song, R. A. Clark, E. F. Bowden and M. J. Tarlov, *J. Phys. Chem.,* 1993, **97**, 6564-6572.

2 Q. Chi, J. Zhang, J. E. T. Andersen and J. Ulstrup, *J. Phys. Chem. B*, 2001, **105**, 4669-4679.

3 P. S. Jensen, Q. Chi, F. B. Grumsen, J. M. Abad, A. Horsewell, D. J. Schiffrin and J. Ulstrup, *J. Phys. Chem. C*, 2007, **111**, 6124 - 6133.

4 (a) S. Imabayashi, T. Mita and T. Kakiuchi, *Langmuir,* 2005, **21**, 1470-1474. (b) E. Della-Pia, Q. Chi, J. E. Macdonald, J. Ulstrup, D. Jones and

M. Eliott, *Nanoscale,* 2012, **4**, 7106 – 7113. (c) E. Della-Pia, Q. Chi, D. Jones, J. E. Macdonald, J. Ulstrup and M. Eliott, *Nano Lett,* 2011, **11**, 176 – 182.

5 (a) Q. Chi, O. Farver and J. Ulstrup, *Proc. Natl. Acad. Sci. USA*, 2005*,* **102**, 16203-16208. (b) P. S. Jensen, Q. Chi, J. Zhang and J. Ulstrup, *J. Phys. Chem. C*, 2009, **113***,* 13993-14000.

6 J. D. Zhang, H. E. M. Christensen, B. L. Ooi and J. Ulstrup, *Langmuir,* 2004, **20**, 10200-10207.

7 (a) J. Zhang, A. C. Welinder, A. G. Hansen, H. E. M. Christensen and J. Ulstrup, *J. Phys. Chem. B*, 2003, **107**, 12480-12484. (b) V. Climent, J. Zhang, E. P. Friis, L. H. Østergaard and J. Ulstrup, *J. Phys. Chem. C*, 2012, **116**, 1232-1243.

8 A. A. Karyakin, O. V. Gitelmacher and E. E. Karyakina, *Anal. Chem.*, 1995, **67**, 2419-2423.

9 Q. Chi and S. J. Dong, *Anal. Chim. Acta*, 1995, **310**, 429-436.

10 Y. N. Zhang, Z. Y. Chu, L. Shi and W. Q. Jin, *Electrochim. Acta*, 2011, **56**, 8163-8167.

11 F. Ricci and G. Palleschi, *Biosens. Bioelectron.*, 2005, **21**, 389-407.

12 Y. Q. Miao, J. R. Chen, X. H. Wu, K. M. Fang, A. P. Jia and J. W. Liu, *J. Nanosci. Nanotech.*, 2007, **7**, 2877-2882.

13 A. A. Karyakin and E. E. Karyakina, *Russian Chem. B*, 2001, **50**, 1811-1817.

14 H. Razmi, R. Mohammad-Rezaei and H. Heidari, *Electroanalysis*, 2009, **21**, 2355-2362.

15 N. Bowden, A. Terfort, J. Carbeck and G. M. Whitesides, *Science*, 1997, **276**, 233-235.

16 F. Matemadombo, P. Westbroek, T. Nyokong, K. Ozoemena, K. De Clerck and P. Kiekens, *Electrochim. Acta*, 2007, **52**, 2024-2031.

17 Q. Chi, J. Zhang, J. U. Nielsen, E. P. Friis, Ib. Chorkendorff, G. W. Canters, J. E. T. Andersen and J. Ulstrup, *J. Am. Chem. Soc.*, 2000*,* **122**, 4047-4055.

18 J. Zhang, Q. Chi, J. U. Nielsen, E. P. Friis, J. E. T. Andersen and J. Ulstrup, *Langmuir*, 2000, **16**, 7229-7237.

19 J. Zhang, Q. Chi, A. M. Kuznetsov, H. E. M. Christensen, J. E. T. Andersen and J. Ulstrup, *J. Phys. Chem. B*, 2002*,* **106**, 1131-1152.

20 J. Zhang, A. M. Kuznetsov, I. G. Medvedev, Q. Chi, T. Albrecht, P. S. Jensen and J. Ulstrup, *Chem. Rev.*, 2008, **108**, 2737-2791.

21 Q. Chi, J. Zhang, T. Arstan, L. Borg, G. W. Pedersen, H. E. M. Christensen and J. Ulstrup, *J. Phys. Chem. B*, 2010, **114**, 5617-5624.

22 X. Hao, N. Zhu, T. Gschneidtner, E. O. Jonsson, J. Zhang, K. Moth-Poulsen, H. D. Wang, K. S. Thygesen, K. W. Jacobsen, J. Ulstrup and Q. Chi, *Nat. Commun.,* 2013, **4,** 2121.

23 D. Zhang, K. Zhang, Y. L. Yao, X. H. Xia and H. Y. Chen, *Langmuir*, 2004, **20**, 7303-7307.

24 S. X. Wang, Y. Zhou, H. Niu and X. Z. Zhang, *Curr. Appl. Phys.*, 2011, **11**, 1337-1342.

25 Y. Lvov, K. Ariga, I. Ichinose and T. Kunitake, *J. Am. Chem. Soc.*, 1995, **117**, 6117-6123.

26 K. Gerasopoulos, E. Pomerantseva, M. McCarthy, A. Brown, C. S. Wang, J. Culver and R. Ghodssi, *ACS Nano*, 2012, **6**, 6422-6432.

27 Y. Chen, X. J. Yang, L. R. Guo, J. Li, X. H. Xia and L. M. Zheng, *Ana. Chim. Acta*, 2009, **644**, 83-89.

28 R. P. Liang, H. Z. Peng and J. D. Qiu, *J. Colloid Interface Sci.*, 2008, **320**, 125-131.

29 R. Villalonga, P. Diez, P. Yanez-Sedeno and J. M. Pingarrón, *Electrochim. Acta*, 2011, **56**, 4672-4677.

30 P. Diez, C.-G. Piuleac, P. Martinez-Ruiz, S. Romano, M. Gamella, R. Villalonga and J. M. Pingarrón, *Anal. Bioanal. Chem,* 2013, **405**, 3773-3781.

31 E. Araque, C. B. Arenas, M. Gamella, J. Reviejo, R. Villalonga and J. M. Pingarrón, *J. Electroanal. Chem.,* 2014, **717/718**, 96-102.

32 E. Araque, R. Villalonga, M. Gamella, P. Martinez-Ruiz, J. Reviejo and J. M. Pingarrón, *J. Mater. Chem. B,* 2013, **1**, 2289-2296.

33 N. A. Pchelintsev, A. Vakurov and P. A. Millner, *Sens. Actuators B: Chem.,* 2009, **138**, 461-466.

34 N. A. Hirst, L. D. Hazelwood, D. G. Jayne, P. A. Millner, *Sens. Actuators B: Chem.,* 2013, **186**, 674-680.

35 C. Shan, L. Wang, D. Han, F. Li, Q. Zhang, X. Zhang, L. Niu, *Thin Solid Films*, 2013, **534**, 572-576.

36 L. Zhang, A. Zhang, D. Du and Y. Li, *Nanoscale*, 2012, **4**, 4674-4679.

37 Y. Zhang, H. Chen, X. Gao, Z. Chen, X. Lin, *Biosens. Bioelectron.,* 2012, **35**, 277-283.

38 A. J. Lomant and G. Fairbanks, *J. Mol. Biol.*, 1976, **104**, 243-261.

39 M. Darder, K. Takada, F. Pariente, E. Lorenzo and H. D. Abruna, *Anal. Chem.*, 1999, **71**, 5530-5537.

40 S. Imabayashi, M. Iida, D. Hobara, Z. Q. Feng, K. Niki and T. Kakiuchi, *J. Electroanal. Chem.* 1997, **428**, 33-38.

41 X. J. Chen, Z. X. Chen, R. Tian, W. Yan and C. Yao, *Ana. Chim. Acta*, 2012, **723**, 94-100.

42 T. Kakiuchi, H. Usui, D. Hobara and M. Yamamoto, *Langmuir*, 2002, **18**, 5231-5238.

43 C. A. Widrig, C. Chung and M. D. Porter, *J. Electroanal. Chem.*, 1991, **310**, 335-359.

44 M. M. Walczak, D. D. Popenoe, R. S. Deinhammer, B. D. Lamp, C. K. Chung and M. D. Porter, *Langmuir*, 1991, **7**, 2687-2693.

45 J. Zhang, A. Bilič, J. R. Reimers, N. S. Hush and J. Ulstrup, *J. Phys. Chem. B*, 2005**, 109***,* 15355-15367.

46 A. J. Bard and L. N. Faulkner, Eds. *Electrochemical Methods*, 2nd ed., John Wiley and Sons Ltd, Chichester, UK and New York, USA: New York, 2001.

47 E. Laviron, *J. Electroanal. Chem.*, 1979, **101**, 19-28.

48 A. A. Kornyshev, A. M. Kunetsov, E. Spohr and J. Ulstrup, *J. Phys. Chem. B*, 2003, **107**, 3351-3366.

49 K. Doblhofer, D. Nölte and J. Ulstrup, *Ber. Bunsenges. Physik. Chem.*, 1978, **82**, 403-408.

50 P. Daum, J. R. Lenhard, D. Rolinson and R.W. Murray, *J. Am. Chem. Soc.*, 1980, **102**, 4649-4653.

51 J. W. Schultze, L. Elfenthal, K. Leitner and O. Meyer, *Mater. Sci. Eng.,* 1987, **90**, 253-262.

52 M. H. Jensen, P. Osvath, A. M. Sargeson and J. Ulstrup, *J. Electroanal. Chem.*, 1994, **377**, 131-141.

53 K. Aoki, K. Tokuda and H. Matsuda, *J. Electroanal. Chem.*, 1983, **146**, 417-424.

54 K. Aoki, K. Tokuda and H. Matsuda, *J. Electroanal. Chem.*, 1984, **160**, 33-45.

55 A. T. Hubbard and F. C. Anson, *Anal. Chem*., 1966, **38**, 58-61.

56 I. Almeida, A. C. Cascalheira and A. S. Viana, *Electrochim. Acta*, 2010, **55**, 8686-8695.

57 H. J. Hecht, H. M. Kalisz, J. Hendle, R. D. Schmid and D. Schomburg, *J. Mol. Biol*., 1993, **229**, 153-172.

58 H. Muguruma, Y. Kase, N. Murata and K. Matsumura, *J. Phys. Chem. B*, 2006, **110**, 26033-26039.

59 J. D. Qiu, H. Z. Peng, R. P. Liang and M. Xiong, *Electroanalysis*, 2007, **19**, 1201-1206.
60 N. Zhu, S. Han, S. Gan, J. Ulstrup and Q. Chi, *Adv. Funct. Mater.*, 2013, **23**, 5297-5306.
61 N. Zhu, Ph.D. Thesis, Technical University of Denmark, 2800 Kongens Lyngby, Denmark, 2013.
62 Q. Chi, J. Zhang, P. S. Jensen, H. E. M. Christensen and J. Ulstrup, *Faraday Discussion* 2006, **131**, 181-195.

TOC Graphic

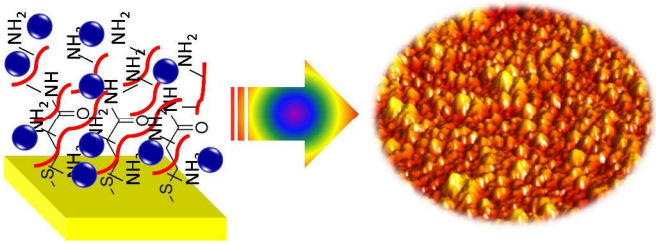

Synopsis: **Three-dimensional interfacial nanocomposite consisting of a polymer matrix, electroactive nanoparticles and enzyme is synthesized on electrode surfaces via surface self-assembly chemistry. The nanocomposite shows promising observations for achieving fast electron transfer and efficient electrocatalysis.**